NuSTAR AND *CHANDRA* INSIGHT INTO THE NATURE OF THE 3–40 keV NUCLEAR EMISSION IN NGC 253

B. D. Lehmer[1,2], D. R. Wik[2], A. E. Hornschemeier[2], A. Ptak[2], V. Antoniou[3], M. K. Argo[4], K. Bechtol[5], S. Boggs[6],
F. E. Christensen[7], W. W. Craig[6,8], C. J. Hailey[9], F. A. Harrison[10], R. Krivonos[6], J.-C. Leyder[2,11],
T. J. Maccarone[12,13], D. Stern[14], T. Venters[2], A. Zezas[15], AND W. W. Zhang[2]

[1] The Johns Hopkins University, Homewood Campus, Baltimore, MD 21218, USA
[2] NASA Goddard Space Flight Center, Code 662, Greenbelt, MD 20771, USA
[3] Department of Physics and Astronomy, Iowa State University, 12 Physics Hall, Ames, IA 50011, USA
[4] ASTRON, the Netherlands Institute for Radio Astronomy, Postbus 2, 7990 AA, Dwingeloo, The Netherlands
[5] Kavli Institute for Cosmological Physics, Chicago, IL 60637, USA
[6] Space Sciences Laboratory, University of California, Berkeley, CA 94720, USA
[7] DTU Space—National Space Institute, Technical University of Denmark, Elektrovej 327, DK-2800 Lyngby, Denmark
[8] Lawrence Livermore National Laboratory, Livermore, CA 94720, USA
[9] Columbia Astrophysics Laboratory, Columbia University, New York, NY 10027, USA
[10] Caltech Division of Physics, Mathematics and Astronomy, Pasadena, CA 91125, USA
[11] Universities Space Research Association, Columbia, MD 21044, USA
[12] School of Physics and Astronomy, University of Southampton, Highfield SO17 IBJ, UK
[13] Department of Physics, Texas Tech University, Box 41051, Lubbock, TX 79409-1051, USA
[14] Jet Propulsion Laboratory, California Institute of Technology, Pasadena, CA 91109, USA
[15] Physics Department, University of Crete, Heraklion, Greece

ABSTRACT

We present results from three nearly simultaneous *Nuclear Spectroscopic Telescope Array* (*NuSTAR*) and *Chandra* monitoring observations between 2012 September 2 and 2012 November 16 of the local star-forming galaxy NGC 253. The 3–40 keV intensity of the inner $\sim$20 arcsec ($\sim$400 pc) nuclear region, as measured by *NuSTAR*, varied by a factor of $\sim$2 across the three monitoring observations. The *Chandra* data reveal that the nuclear region contains three bright X-ray sources, including a luminous ($L_{2-10\,{\rm keV}} \sim$ few $\times 10^{39}$ erg s^{-1}) point source located $\sim$1 arcsec from the dynamical center of the galaxy (within the 3σ positional uncertainty of the dynamical center); this source drives the overall variability of the nuclear region at energies $\gtrsim$3 keV. We make use of the variability to measure the spectra of this single hard X-ray source when it was in bright states. The spectra are well described by an absorbed ($N_{\rm H} \approx 1.6 \times 10^{23}$ cm^{-2}) broken power-law model with spectral slopes and break energies that are typical of ultraluminous X-ray sources (ULXs), but not active galactic nuclei (AGNs). A previous *Chandra* observation in 2003 showed a hard X-ray point source of similar luminosity to the 2012 source that was also near the dynamical center ($\theta \approx 0.4$ arcsec); however, this source was offset from the 2012 source position by $\approx$1 arcsec. We show that the probability of the 2003 and 2012 hard X-ray sources being unrelated is $\gg$99.99% based on the *Chandra* spatial localizations. Interestingly, the *Chandra* spectrum of the 2003 source (3–8 keV) is shallower in slope than that of the 2012 hard X-ray source. Its proximity to the dynamical center and harder *Chandra* spectrum indicate that the 2003 source is a better AGN candidate than any of the sources detected in our 2012 campaign; however, we were unable to rule out a ULX nature for this source. Future *NuSTAR* and *Chandra* monitoring would be well equipped to break the degeneracy between the AGN and ULX nature of the 2003 source, if again caught in a high state.

Key words: galaxies: active – galaxies: individual (NGC 253) – galaxies: star formation – galaxies: starburst – X-rays: galaxies

Online-only material: color figures

1. INTRODUCTION

Over the last few decades, imaging and spectroscopy in the 0.3–10 keV bandpass has undergone dramatic improvements thanks to advancements from a progression of X-ray observatories. Due to its proximity and starburst nature, the nearby galaxy NGC 253 ($D = 3.9$ Mpc based on the tip of the red giant branch; Karachentsev et al. 2004) has been an ideal target for studying X-ray emission from regions more actively star-forming than the Milky Way and other Local Group galaxies (e.g., Fabbiano & Trinchieri 1984; Ptak et al. 1997; Vogler & Pietsch 1999; Pietsch et al. 2000, 2001; Strickland et al. 2000; Weaver et al. 2002; Bauer et al. 2007, 2008).

Studies of NGC 253 have revealed a diversity of X-ray emitting populations throughout the galaxy. A few dozen X-ray point sources have been detected across the optical extent of the disk (e.g., Pietsch et al. 2001). A thin $\sim$0.4 keV plasma extends several arcminutes along the plane of the disk, and $\sim$1 keV gas has been observed in a collimated kpc-scale outflow emanating from the nuclear starburst (e.g., Strickland et al. 2000; Bauer et al. 2008; Mitsuishi et al. 2013). The inner nuclear region has been resolved by *Chandra* into a few bright point sources within a $\approx$60 arcsec^2 region (i.e., the inner $\approx$150 pc). In this region, a complex line structure of Fe K has been resolved into at least three spectral components due to Fe I at 6.4 keV, Fe XXV at 6.7 keV, and Fe XXVI at 7.0 keV, potentially powered by the combination of an obscured active galactic nucleus (AGN), supernova (SN) remnants, and/or X-ray binaries (Mitsuishi et al. 2011). The point sources include individual X-ray binaries and/or the collective emission from sources within star-forming

clouds (e.g., SN remnants and X-ray binaries), as well as a hard X-ray point source (appearing at energies $\gtrsim 2$ keV) that is located within the 1.2 arcsec 3σ uncertainty radius of the dynamical center of the galaxy (Müller-Sánchez et al. 2010). The central hard X-ray point source has been speculated to be either an obscured ($N_{\rm H} > 10^{23}$ cm^{-2}), low-luminosity ($L_{2-10\,{\rm keV}} \sim$ few $\times 10^{39}$ erg s^{-1}) AGN or a super star cluster lit up by SN and/or SN remnants.

High-resolution studies of the nuclear region of NGC 253 at other wavelengths have revealed a multitude of compact sources within the inner ~ 200 pc (~ 10 arcsec) of the nucleus. The star formation rate (SFR) within this region, based on free–free emission, is estimated to be $\sim 2\ M_\odot$ yr^{-1} (Rodríguez-Rico et al. 2006), perhaps larger than that of the entire Milky Way (SFR $\approx$ 1–2 $M_\odot$ yr^{-1}; Hammer et al. 2007). The central black hole mass has been estimated to be $\approx 5 \times 10^6\ M_\odot$ based on kinematics of the H53α (43 GHz) and H92α (8.31 GHz) recombination lines within the central 18 pc (0.4 arcsec) of the nucleus (Rodríguez-Rico et al. 2006). Within ~ 1 arcsec of the dynamical center are two radio sources, TH2 and TH4, which are separated by 0.36 arcsec and have both been AGN candidates and candidate markers of the galactic center (Ulvestad & Antonucci 1997). TH2 is the brightest 15–22 GHz source in the region and has historically been adopted as the location of the galactic center. The nature of TH2 is still unknown, as the radio spectrum is consistent with both a low-luminosity AGN (LLAGN) and a very compact SN remnant (e.g., Brunthaler et al. 2009). TH4 has been identified as a water-vapor maser source (e.g., Hofner et al. 2006), which initially suggested an AGN origin. However, continuum and maser line imaging with the Very Large Array and Very Long Baseline Array (VLBA) showed that there was no strong continuum point source on arcsecond to milliarcsecond scales, suggesting that the masing source is most likely to originate from star formation processes and not an LLAGN (Brunthaler et al. 2009). Subarcsecond near-IR imaging with the Very Large Telescope adaptive optics system found several star-forming regions in the near vicinity of the nucleus; however, no counterparts were found to TH2 and TH4, again limiting the viability of an AGN presence in NGC 253 (Fernández-Ontiveros et al. 2009). The above studies have revealed that the central nuclear region is almost certainly dominated by star formation processes in the radio and near-IR; however, definitively distinguishing between the starburst and AGN nature in the X-ray band has not yet been possible.

In this paper, we present new insight into the nature of the nuclear region in NGC 253 as a result of a monitoring campaign consisting of three nearly simultaneous observations with the *Nuclear Spectroscopic Telescope Array* (*NuSTAR*; Harrison et al. 2013) and *Chandra*. Within the unique energy range constrained by *NuSTAR*, ≈ 10–40 keV for NGC 253, the spectrum associated with a heavily obscured or LLAGN will differ dramatically from non-AGN spectra (e.g., SN, SN remnants, X-ray binaries, and ultraluminous X-ray sources (ULXs)). Our monitoring campaign therefore allowed us to simultaneously constrain the spectrum of the central nuclear region up to ≈ 40 keV and sensitively measure the locations and contributions of the multiple X-ray sources associated with the same region using subarcsecond imaging with *Chandra*. The Galactic column density in the direction of NGC 253 is 1.4×10^{20} cm^{-2} (Stark et al. 1992). All X-ray fluxes and luminosities quoted here have been corrected for Galactic absorption. At the distance of NGC 253, 1 arcsec corresponds to a physical distance of 19 pc. Unless stated otherwise, quoted un-
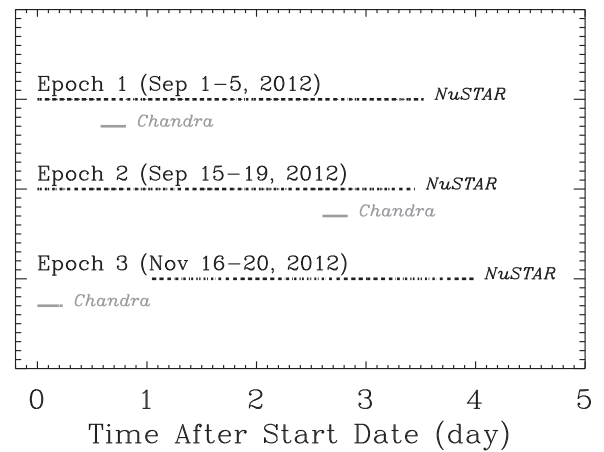

Figure 1. Relative *NuSTAR* (black lines) and *Chandra* (gray lines) observational coverage for each of the three epochs. For clarity, we have annotated the total range of observational dates for each epoch. The apparently broken up *NuSTAR* observational intervals are due primarily to Earth occultations and passages through the SAA.

certainties throughout this paper correspond to 90% confidence intervals.

2. OBSERVATIONS AND DATA REDUCTION

Our nearly simultaneous *NuSTAR* and *Chandra* observations of NGC 253 were conducted in three observational epochs that began on 2012 September 1, 2012 September 15, and 2012 November 16; hereafter, epochs 1, 2, and 3, respectively. During each epoch, we obtained integrated exposures of ≈ 165 ks with *NuSTAR* and ≈ 20 ks with *Chandra*. In Figure 1, we show the relative *NuSTAR* and *Chandra* observational coverage for the three epochs. We note that due to Earth occultations and passages through the South Atlantic Anomaly (SAA), the *NuSTAR* on target observational efficiency was 54%–63% (see Harrison et al. 2013 for further details). Therefore, each *NuSTAR* observation was completed over 260–306 ks (i.e., 3–3.5 days; see Figure 1). For epochs 1 and 2, the shorter *Chandra* exposure was conducted within the *NuSTAR* observational interval; however, for epoch 3, the start of the *Chandra* observation preceded that of the *NuSTAR* observation by ≈ 1 day. Additional nearly simultaneous observations were taken with the VLBA at 1.4 GHz in 8 hr exposures. However, due to their depth and frequency, these observations did not yield detections of the candidate nuclear sources TH2 and TH4, and are therefore not discussed further here. Details regarding the VLBA data and NGC 253 galaxy-wide radio population properties will be presented in a future paper (M. K. Argo et al., in preparation).

Each ≈ 165 ks *NuSTAR* exposure was conducted using both telescopes, A + B, which collected 3–80 keV photons from the same $12' \times 12'$ region centered on the nucleus of NGC 253. We performed *NuSTAR* data reduction using `HEASoft 6.12` and `nustardas` v. 0.9.0 with `CALDB` v. 20121126. We processed level 1 data to level 2 products by running `nupipeline`, which performs a variety of data reduction steps, including filtering out bad pixels, screening for cosmic rays and observational intervals when the background was too high (e.g., during passes through the SAA), and projecting accurately the events to sky coordinates by determining the optical axis position and correcting for the dynamic relative offset of the optics bench to the focal plane bench due to motions of the 10 m mast that connects these two benches. In Figure 2(a), we display a

2
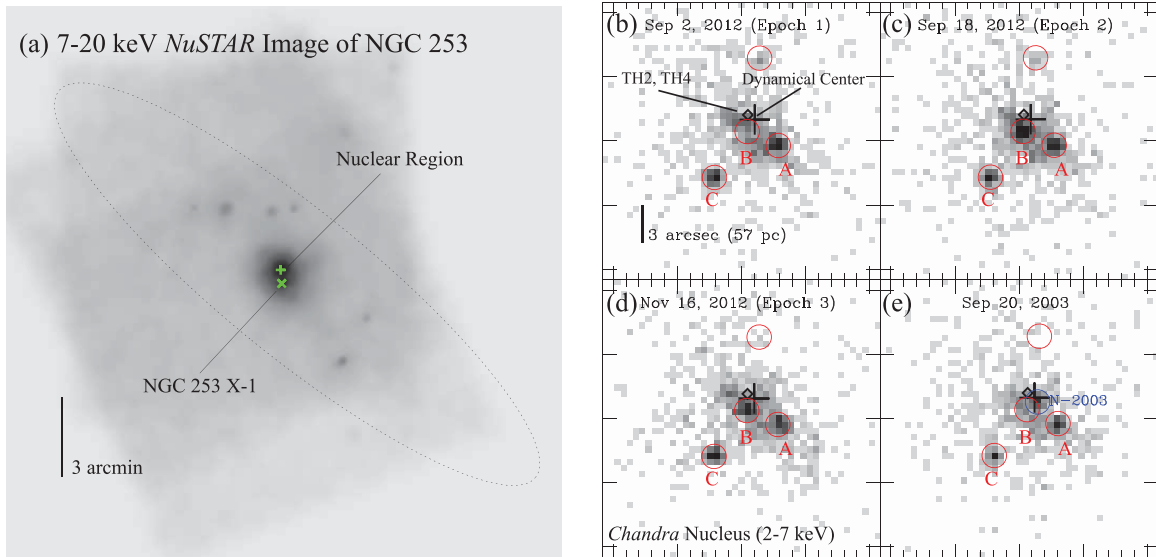
Figure 2. (a) Adaptively smoothed 7–20 keV *NuSTAR* image of NGC 253. The dotted ellipse represents the optical extent of the galaxy (major axis of ≈24 arcmin) at a surface density of $\mu_B \approx 24$ mag arcsec^{-2} (Pence 1980). The locations of the dynamical center (green "+" symbol) and bright off-nuclear source NGC 253 X-1 (green "×" symbol) have been highlighted. (b)–(e) The 2–7 keV *Chandra* images of the inner ≈22 × 22 arcsec^2 region of the nucleus for epochs 1, 2, 3, and the 2003 observation (limited to the first ≈20 ks), respectively. Red circles (≈1 arcsec in radius) represent the average positions of each *Chandra* source in the three 2012 epochs; the three bright nuclear sources have been labeled "A"–"C." The obscured source found in the nuclear region during our 2012 campaign is source B, located at $(\alpha, \delta)_{J2000} = 00^h47^m33^s.18, -25°17'18''.48$, while the blue circle in panel (e) indicates the location of the obscured source detected in 2003, "N-2003" $((\alpha, \delta)_{J2000} = 00^h47^m33^s.12, -25°17'17''.87)$. In each panel, the location of TH2 and TH4 have been shown as a single diamond, and the dynamical center of the galaxy is indicated by a 2.4 arcsec × 2.4 arcsec cross, corresponding to the 3σ astrometric uncertainty (from Müller-Sánchez et al. 2010).

(A color version of this figure is available in the online journal.)

7–20 keV *NuSTAR* image of NGC 253, which was constructed by merging data from all three observational epochs.

All three of the ≈20 ks *Chandra* exposures were conducted using single $16'.9 \times 16'.9$ ACIS-I pointings (ObsIDs: 13830, 13831, and 13832) with the approximate position of the nucleus set as the aim point. For our data reduction, we used CIAO v. 4.4 with CALDB v. 4.5.0. We reprocessed our event lists, bringing level 1 to level 2 using the script chandra_repro, which identifies and removes events from bad pixels and columns, and filters event lists to include only good time intervals without significant flares and non-cosmic-ray events corresponding to the standard *ASCA* grade set (grades 0, 2, 3, 4, and 6). We constructed an initial *Chandra* source catalog by searching a 0.5–7 keV image with wavdetect (run with a point-spread function (PSF) map created using mkpsfmap), which was set at a false-positive probability threshold of 2×10^{-5} and run over seven scales from 1 to 8 (spaced out by factors of $\sqrt{2}$ in wavelet scale: 1, $\sqrt{2}$, 2, $2\sqrt{2}$, 4, $4\sqrt{2}$, and 8). Each initial *Chandra* source catalog was cross-matched to an equivalent catalog, which we created following the above procedure using a moderately deep (≈80 ks) *Chandra* ACIS-S exposure from 2003 September 20 (ObsID: 3931). The 2003 observation is the deepest *Chandra* image available for NGC 253 and has an aim point close to those of the three 2012 observations. For the purpose of comparing point sources in the 2012 observations with those of the deep 2003 exposure, we chose to register the 2012 aspect solutions and event lists to the 2003 frame using CIAO tools reproject_aspect and reproject_events, respectively. The resulting astrometric reprojections gave very small astrometric adjustments, including linear translations of $\delta x = -0.49$ to $+0.37$ pixels and $\delta y = +0.28$ to 0.37 pixels, rotations of -0.026 to -0.004 deg, and pixel scale stretch factors of 0.999963–1.000095. The final pixel scale of all observations was 0.492 arcsec pixel^{-1}.

Figures 2(b)–(e) show 2–7 keV *Chandra* cutouts of the central nuclear region of NGC 253 for our 2012 campaign and the 2003

observation. These images from our 2012 campaign clearly illustrate that the nuclear region can be resolved into three bright 2–7 keV point sources, A, B, and C (see Figures 2(b)–(e)), which appear as a single point source with *NuSTAR*'s ≈18 arcsec FWHM PSF (see Figure 2(a)). The source located ≈1 arcsec to the south of the dynamical center (but within the 3σ dynamical center uncertainty radius of 1.2 arcsec), source B $((\alpha, \delta)_{J2000} = 00^h47^m33^s.18, -25°17'18''.48)$, is clearly variable and represents the best candidate in our 2012 observations for a nuclear point source. In the 2003 observation (Figure 2(e)), the nearest nuclear source to source B (offset by ≈1 arcsec) is labeled "N-2003" $((\alpha, \delta)_{J2000} = 00^h47^m33^s.12, -25°17'17''.87)$. Our analyses below focus on uncovering the nature of source B and N-2003.

3. RESULTS AND DISCUSSION

3.1. Spectral Properties of the Nuclear Region

We began by extracting the *NuSTAR* spectra from the nuclear region of NGC 253 for each of the three observations. In order to encompass a large fraction of the source counts in the nuclear region, while minimizing contamination from nearby unrelated sources, we chose to extract the spectra using circular regions with radii of 20 arcsec (≈400 pc), somewhat larger than the *NuSTAR* half width at half maximum (i.e., ≈9 arcsec). This choice of aperture encompasses 32% of the *NuSTAR* PSF (half-power radius 29 arcsec). Background spectra were extracted from larger apertures (17–37 arcmin^2 depending on the observational epoch), which were defined by eye as source-free regions. We note that NGC 253 X-1, the bright off-nuclear source ≈30 arcsec to the south of the nucleus, is a ULX with $L_{2-10 keV} \approx (2-3) \times 10^{39}$ erg s^{-1} (based on analysis below) and provides some non-negligible contribution to the nuclear region spectra (see Figure 2(a)). To estimate these contributions, we extracted spectra of this source using 20 arcsec
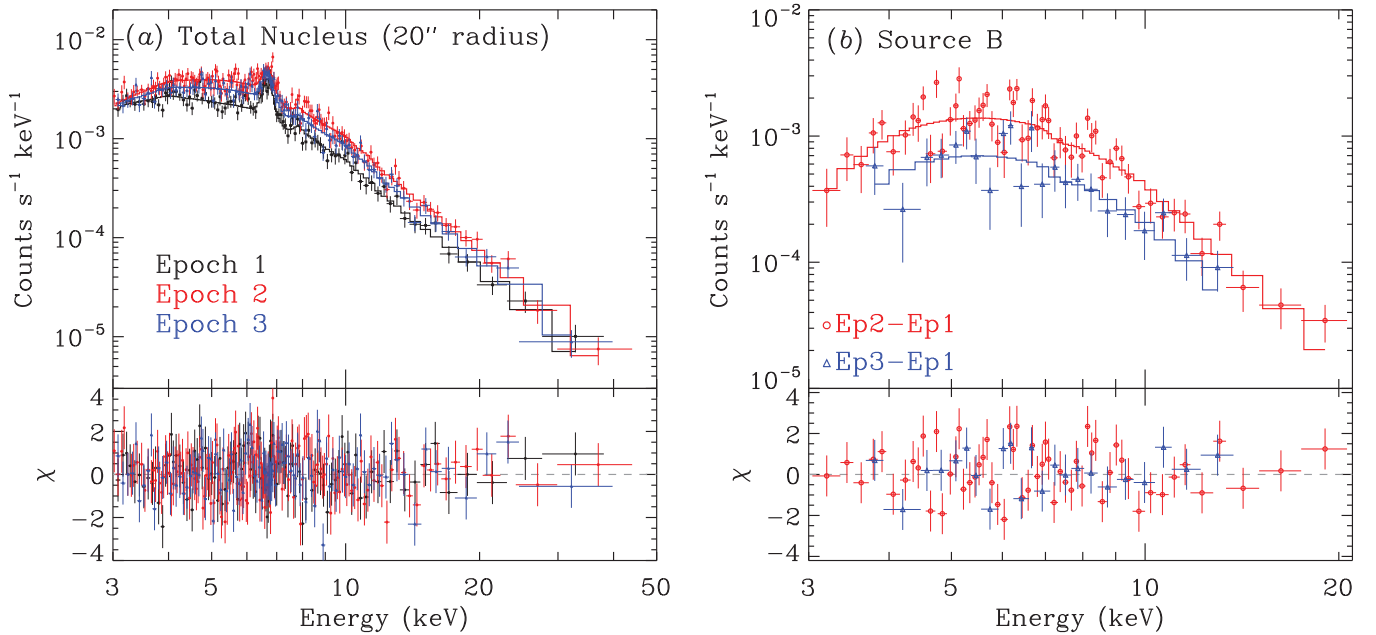
Figure 3. (a) *NuSTAR* spectra of the central nuclear region of NGC 253 for the three observational epochs. The spectra are all simultaneously fit (solid curves) by the sum of a non-variable component, including a $\approx$3.6 keV hot plasma (`apec`) model plus an unabsorbed `power-law` model ($\Gamma_{\rm non-var} \approx 2.1$), and an absorbed ($N_{\rm H} \approx 2.5 \times 10^{23}$ cm^{-2}) variable `power-law` component ($\Gamma_{\rm var} \approx 3.0$). The power-law components account for emission from persistent and variable X-ray binaries and the putative AGN. (b) *NuSTAR* difference spectra of source B based on the difference between epochs 2 and 1 and epochs 3 and 1. The difference spectra were fit by a moderately absorbed ($N_{\rm H} \approx 1.6 \times 10^{23}$ cm^{-2}) broken power-law model with $\Gamma_1 \approx 2.4$, $E_{\rm break} \approx 7.9$ keV, and $\Gamma_2 \approx 3.9$. Again, the only difference between fits is the normalization of the power-law component, indicating that the absorption did not change substantially between observations. The spectral shape is consistent with parameters measured for ULXs, but not AGNs.

(A color version of this figure is available in the online journal.)

radii circular apertures. The spectra of NGC 253 X-1 were fit using `xspec` v.12.7.1 (Arnaud 1996) and a broken power-law model `bknpower` with varying normalization. We found a best-fit low-energy slope of $\Gamma_1 = 2.1 \pm 0.1$, break energy $E_{\rm break} = 6.8 \pm 0.2$ keV, and high-energy slope $\Gamma_2 = 4.1 \pm 0.1$; no absorption was required in any of these fits. These values are similar to those of ULXs studied in detail by Gladstone et al. (2009), which have $L_{\rm 2-10\,keV} = (1-14) \times 10^{39}$ erg s^{-1}, and are fit well by broken power-law models with $\Gamma_1 = 1-3$, $E_{\rm break} = 3-8$ keV, and $\Gamma_2 = 2-7$. Using a PSF model, we estimate that the contributions of NGC 253 X-1 to the nuclear region spectra are small ($\lesssim$10% for all three epochs). From our best-fit spectral models for NGC 253 X-1, we constructed fake background spectra corresponding to its contributions to the nuclear region spectra. These were used when performing spectral fits to the nuclear region itself (see below). To test the robustness of this procedure, we measured the spectral contributions from the wings of the *nuclear region* PSFs to see if they influenced the extracted spectra of NGC 253 X-1. Once contributions from the nuclear region PSFs were subtracted, we found only very small differences (at the $\lesssim$7% level) in spectral parameters and normalizations derived for NGC 253 X-1. Such differences translate into $\lesssim$1% differences in the derived spectral properties of the nuclear region itself, well below the precision of our measurements. We therefore conclude that our procedure for estimating the contributions of NGC 253 X-1 to the nuclear region is robust.

In Figure 3(a), we present the *NuSTAR* spectra of the central nuclear region for the three epochs. We do not include the *Chandra* spectra of the nuclear point sources here, since a direct matching between the multiple components that lie within the *NuSTAR* beam is complex and unnecessary for understanding

the hard X-ray properties of the nuclear region that we are interested in here. We know that the *NuSTAR* emission from the central nuclear region is a combination of hot plasma, as well as non-variable and variable power-law sources (i.e., X-ray binaries and a putative AGN). We therefore fit the spectra (with background and NGC 253 X-1 contributions subtracted) of all three epochs simultaneously using an `apec` plasma model to account for the hot gas plus two `power-law` components that account for the non-variable and variable power-law sources, the latter of which we expect to be primarily due to source B. We note that the X-ray emitting gas is likely to be complex and contain multiple components (e.g., Pietsch et al. 2001; Mitsuishi et al. 2013). However, since these components have their strongest influence at energies $\lesssim$1–2 keV, we chose to utilize a single hot plasma to account for the Fe-line emission. Such a component is expected to account for hot gas in the core of the starburst associated with SN remnants (see, e.g., Pietsch et al. 2001). Our adopted model provides a good fit to the data (see Figure 3(a)) by simply varying only the normalization of the power law associated with variable sources like source B. Our best-fit model parameters include an `apec` plasma with $kT = (3.6 \pm 0.3)$ keV, a non-variable unobscured power-law component with $\Gamma_{\rm non-var} = 2.1 \pm 0.1$, and an absorbed ($N_{\rm H} = [2.5 \pm 0.4] \times 10^{23}$ cm^{-2}) variable power law with $\Gamma_{\rm var} = 3.4 \pm 0.2$. The 7–20 keV flux of the nuclear region was factors of 1.69 ± 0.11 and 1.39 ± 0.08 (1σ errors) times higher in epochs 2 and 3, respectively, than its flux in epoch 1 ($f_{\rm 7-20\,keV}^{\rm epoch1} = 7.5 \times 10^{-13}$ erg cm^{-2} s^{-1}).

We also tried accounting for the variability by allowing the variable power-law absorption column, photon index, and normalization components to vary in different combinations. Holding the normalization constant and varying the column

density alone provided an acceptable fit and resulted in column densities $\gtrsim 2.9 \times 10^{23}$ cm^{-2} and $\Gamma_{\rm var} \approx 3.7$. Holding the normalization and varying only the photon index between epochs did not provide an acceptable fit to the data. Finally, varying the column density, photon index, and normalization components simultaneously provided a good fit to the data, and indicate that the variable component had high absorption columns ($N_{\rm H,var} \gtrsim 2.6 \times 10^{23}$ cm^{-2}) and steep photon indices ($\Gamma_{\rm var} \gtrsim 3.6$). None of the above variations improved the quality of the fits to the data over a simple variation in normalization between epochs. This analysis indicates that the 3–40 keV spectral slope is much steeper than that found for typical AGNs ($\Gamma \approx 1.5$–2.2; e.g., Corral et al. 2011; Vasudevan et al. 2013).

3.2. Properties of Source B

As discussed in Section 2 above, the nuclear region of NGC 253 is resolved by *Chandra* into three bright point sources detected at 2–7 keV within a ≈ 60 arcsec^2 region. The *NuSTAR* PSF is too large to spatially distinguish these sources. However, the *NuSTAR* and *Chandra* spectral coverages overlap in the energy range of ≈ 3–7 keV, allowing us to measure indirectly the levels that each source contributes to the *NuSTAR* flux variations. With *Chandra*, we found that only the central source (labeled source "B" in Figures 2(b)–(e)) varied significantly over the three epochs. To estimate the fractional contributions that source B provided to the total *NuSTAR* extraction region spectra, we measured 4–7 keV count rates from source B and a larger nuclear region using circular apertures of 1.0 arcsec and 15 arcsec, respectively. We find that the 4–7 keV flux from the larger nuclear region was factors of 1.6 ± 0.1 and 1.2 ± 0.1 (1σ errors) higher in epochs 2 and 3, respectively, compared with epoch 1; this is consistent with the *NuSTAR* observations over the same energy range, which were 1.58 ± 0.07 and 1.33 ± 0.06 (1σ errors), respectively. Given that the shorter 20 ks (0.23 day) *Chandra* exposures did not cover the entire ≈ 3–3.5 day periods spanned by the *NuSTAR* observations (see Figure 1), this result indicates that the nuclear region was unlikely to vary substantially during each of the observational epochs. We verified this result by inspecting *NuSTAR* light curves of the nuclear region. These light curves were constructed by extracting event lists from a 10 arcsec radius circle centered on the nucleus and measuring the mean count rates of this region in 20 ks bins. We found no signatures of strong variability within each of the three observational epochs. A K-S test revealed that each of the nuclear region light curves were consistent with those expected from constant-intensity sources. We therefore conclude that the nuclear region did not vary substantially on timescales of ≈ 6–48 hr. Our *Chandra* observations indicate that source B itself was brighter in epochs 2 and 3 compared with epoch 1 by factors of 5.2 ± 1.0 and 2.6 ± 0.6 (1σ errors), respectively. Once we subtract the contributions of source B to the total *Chandra* fluxes, contained within the larger *NuSTAR* extraction region, we find no significant remaining variations in the 4–7 keV non-source B emission between all three epochs, indicating that nuclear region variability observed within the *NuSTAR* PSF, at least in the 4–7 keV band, are likely entirely attributable to variations in source B.

Assuming the *NuSTAR* variability is primarily due to variations in source B, we can estimate its spectra by differencing the total nuclear region spectra between bright and faint epochs. Since the variations in the total *NuSTAR* spectra appear to be consistent with only changes in spectral normalization and not shape (see above), we assume that S_i, the total nuclear region

spectrum in epoch i, is described by

$$S_i \equiv S_{\rm const} + c_i S_B, \tag{1}$$

where the constant $S_{\rm const}$ represents all the non-variable emission in the nuclear region (e.g., due to sources A and C, as well as diffuse emission), the constant S_B represents the spectrum of source B, and c_i represents the variable normalization of source B at epoch i. Indeed, Figure 3(b) shows the difference spectra, which are well fit by an absorbed broken power-law model with best-fit $N_{\rm H} = (1.6 \pm 0.5) \times 10^{23}$ cm^{-2}, low-energy slope of $\Gamma_1 = 2.4 \pm 0.5$, break energy $E_{\rm break} = 7.9 \pm 0.9$ keV, and high-energy slope $\Gamma_2 = 3.9 \pm 0.4$ for both cases, with only the normalization varying. Fitting the difference spectra of epoch 2 minus epoch 1 and epoch 3 minus epoch 1 separately yields similar best-fit parameters and no improvement in spectral fit, implying the spectral shape of source B did not vary significantly between epochs 2 and 3. Equation (1) then implies

$$c_i S_B = \frac{S_i - S_1}{1 - c_1/c_i}. \tag{2}$$

From the *Chandra* observations, we know that $c_1/c_2 \approx 0.19$ and $c_1/c_3 \approx 0.38$. We note that no Fe line was necessary in our fits to source B implying that variable Fe emission is not seen in this source. This result alone likely rules out the possibility that source B is a more luminous version of the variable Fe reflection nebulae seen in the Galactic center, since we would expect corresponding variability in the Fe emission line (e.g., Ponti et al. 2010).

Integration of our spectral model and Equation (2) implies the 2–10 keV fluxes of source B were ≈ 7.4 and 3.0×10^{-13} erg cm^{-2} s^{-1}, for observations 2 and 3, respectively. These fluxes correspond to observed 2–10 keV luminosities of $L_{2-10\,\rm keV} \approx 1.4 \times 10^{39}$ and 5.6×10^{38} erg s^{-1}, respectively. The unabsorbed, intrinsic 2–10 keV luminosities are therefore $L_{2-10\,\rm keV} \approx 5.1$ and 2.6×10^{39} erg s^{-1}, respectively. We note that the central black hole of NGC 253 has been estimated to be $\approx 5 \times 10^6 \, M_\odot$ (Rodríguez-Rico et al. 2006). Such a black hole would have an Eddington luminosity of $L_{2-10\,\rm keV}^{\rm Edd} \approx 3 \times 10^{43}$ erg s^{-1}. For this approximation, we assumed a 2–10 keV bolometric correction of ≈ 22.4, which corresponds to the median bolometric correction for local AGNs with $L_{2-10\,\rm keV} \approx 10^{41}$–$10^{46}$ erg s^{-1} (Vasudevan & Fabian 2007). If source B were powered by the black hole, then it would be accreting at $\sim 10^{-4}$ Eddington. AGNs with these levels of $L_{2-10\,\rm keV}/L_{\rm Edd}$ typically have spectral slopes of $\Gamma = 1.4 \pm 0.4$ (e.g., Shemmer et al. 2006; Younes et al. 2011), much shallower than the spectrum measured for source B. This suggests that source B is unlikely to be powered by an LLAGN. Instead, the measured luminosities, lack of variability on the ≈ 5–48 hr timescales, and X-ray spectral shape of source B closely resemble the properties of binaries in the ultraluminous state, which include ULXs that are likely to be stellar-mass black holes accreting above the Eddington limit (e.g., Roberts 2007; Heil et al. 2009; Gladstone et al. 2009). It is therefore likely that source B is a ULX and not an AGN. Given that the number of ULXs in galaxies has been observed to correlate with galaxy-wide SFR (e.g., Mineo et al. 2012), it would not be surprising to find a ULX associated with the nuclear starburst of NGC 253. Indeed, multiple bright point sources and transient ULXs have also been observed in the nuclear starburst in M82 (e.g., Feng & Kaaret 2007). Such a feature may be ubiquitous among starburst galaxies. At distances $\gtrsim 5$–10 Mpc, even *Chandra* may have difficulty in distinguishing between such sources.
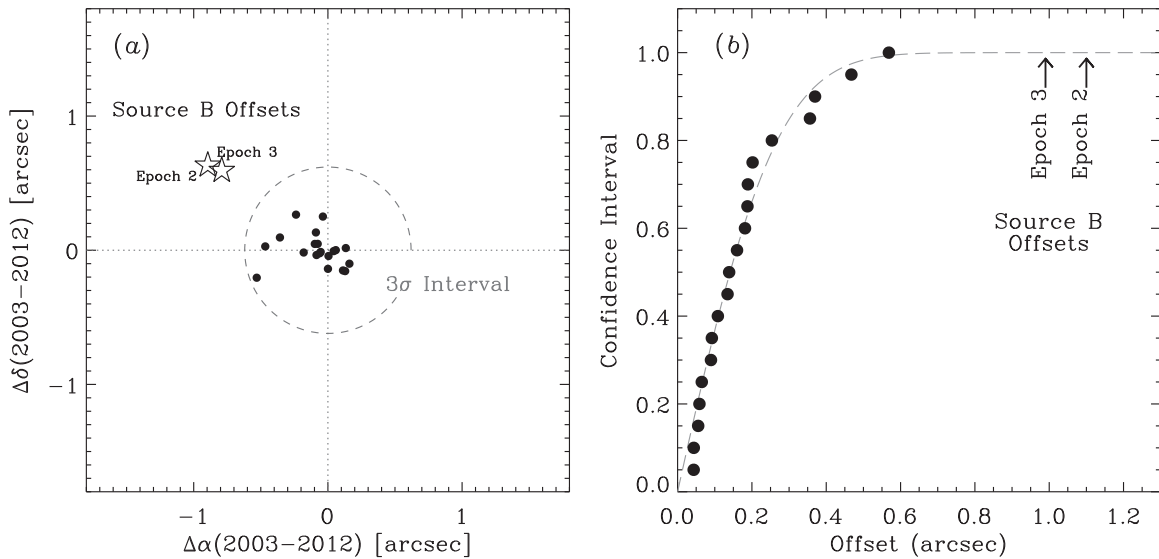
Figure 4. (a) *Chandra* positional offsets in declination $\Delta\delta$ and right ascension $\Delta\alpha$ for 20 NGC 253 point sources detected in 2003 and our three 2012 observations (filled circles). The dashed circle shows the approximate 3σ (99.7%) confidence interval. The offsets between N-2003 and source B in epochs 2 and 3 are indicated with open stars. (b) The cumulative offset distribution for the 20 matched point sources (filled circles) and best-fitting error function (dashed curve). The cumulative offset and best-fitting error functions have been normalized to the maximum error function, which provides direct estimates of confidence intervals. The offsets between N-2003 and source B in epochs 2 and 3 are indicated. Our statistical analysis shows that N-2003 is unrelated to source B at the $\gg$99.99% confidence level.

3.3. Comparisons with the 2003 Chandra Observation

As noted in Section 2 (see also Figure 2(b)), the *Chandra* position of source B is $\sim$1 arcsec from the radio sources TH2 and TH4 (from Ulvestad & Antonucci 1997) and the galactic dynamical center (within the 1.2 arcsec 3σ uncertainty radius; Müller-Sánchez et al. 2010). A similar hard source located $\approx$0.4 arcsec from the dynamical center was previously reported by Müller-Sánchez et al. (2010), based on the *Chandra* observation from 2003. In Figure 2(e), we show the nuclear region image of the first 20 ks of the 2003 observation (to be equivalent to the depth of our 2012 epochs), with the average locations of the 2012 sources circled. It appears that the position of the 2003 hard near-nuclear source (labeled "N-2003" in Figure 2(e)), located at $(\alpha, \delta)_{\rm J2000} = 00^{\rm h}47^{\rm m}33^{\rm s}.12, -25°17'17''.87$, is offset from source B by $\sim$1 arcsec ($\sim$19 pc) in the direction of TH2/TH4, and the dynamical center. We note that three other archival *Chandra* exposures of NGC 253 (ObsID: 790, 969, and 383) were inspected for evidence of N-2003 or source B. Although not formally detected, N-2003 is visually apparent in a 4–7 keV image from the shallower $\approx$14 ks archival observation (ObsID: 969) that was conducted in 1999 December. The moderately deep 45 ks observation (ObsID: 790), also conducted in 1999 December, had an aim point displaced $\approx$5 arcmin from the nuclear region, which effectively blended the PSFs making it impossible to spatially measure whether N-2003 or source B were present. Finally, the $\approx$2 ks exposure conducted in 2000 August (ObsID: 383) was too shallow to detect either N-2003 or source B. We therefore choose to restrict further comparisons of our 2012 observations to the 2003 exposure.

Given the brightness of source B and N-2003 ($\approx$50–300 net counts in the 2–7 keV band) and small off-axis angles with respect to the *Chandra* aim points ($\lesssim$0.5–1 arcmin), we expect the 90% confidence positional errors related to PSF centroiding to be $\approx$0.1–0.2 arcsec (based on Equation (13) of Kim et al. 2007). These positional errors are much smaller than the observed offsets and strongly indicates that the two sources

are unrelated. Although the *Chandra* astrometric frames were aligned to the 2003 observation (see Section 2 for details), some non-negligible error related to image registration is expected. To test further whether the offsets between N-2003 and source B are statistically significant, given our best image registrations, we matched *Chandra* sources detected in the 2003 observation to counterparts detected in each of the three 2012 observations, excluding source B and N-2003. For our matching, we required that sources in each catalog have $\gtrsim$40 net counts in the 2–7 keV band and be located within $\approx$3 arcmin of the nucleus, so that the signal-to-noise ratios and *Chandra* PSFs are comparable to those of N-2003 and source B. Two sources were considered to match if they were separated by $<$2 arcsec. In Figure 4(a), we show the right ascension (α) and declination (δ) offsets for all 20 matches and highlight the offsets between the N-2003 and source B in epochs 2 and 3 (source B was not detected in epoch 1). We find that the offsets between N-2003 and source B are 1.10 and 0.99 arcsec for the epoch 2 and 3 positions, respectively; both are much larger than the maximum offset of the 20 matches (0.6 arcsec). In Figure 4(b), we show the cumulative number of matches as a function of offset with a best-fit error function, which describes well the cumulative offset distribution. The data in Figure 4(b) have been normalized by the error function maximum to allow for direct estimates of the confidence intervals. Our error function suggests that the source B offsets are both significant at the $\gtrsim$99.99% confidence levels. Taken together, we infer that source B is unrelated to N-2003.

The above analysis shows convincingly that N-2003 is unrelated to source B implying that at least one of these sources is not associated with the central black hole. Our spectral constraints, presented in Section 3.2, show that source B is most likely to be a ULX. On the other hand, N-2003 is offset from the dynamical center by only $\approx$0.4 arcsec (i.e., within the 1.2 arcsec 3σ uncertainty of the dynamical center), indicating that it is a better candidate for a "true" nuclear X-ray point source that may be an AGN (see Figure 2(e)). In Figure 5, we show the 3–8 keV *Chandra* spectra of N-2003 and source B (when at its peak in
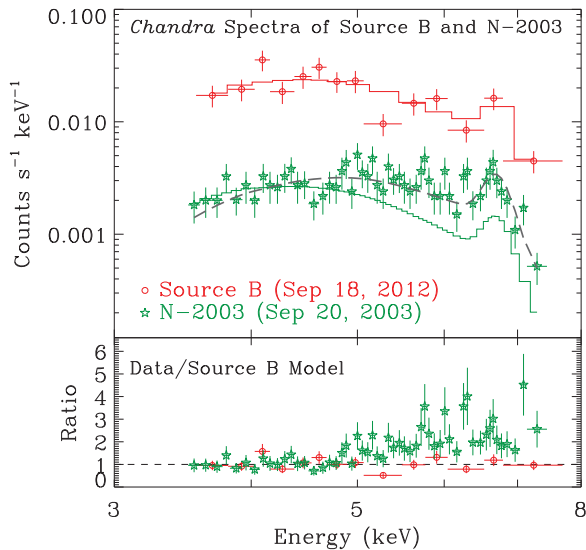
Figure 5. *Chandra* spectra of source B in epoch 2 (red circles) and N-2003 (green stars). For visualization purposes, the normalization of source B has been scaled upward by a factor of four. The solid red curve shows the best-fit spectral model for source B from Figure 3(b), with an Fe component added. The solid green curve shows the same model renormalized to the $\lesssim 5$ keV spectrum of N-2003. The bottom panel displays the ratio between the data and the 2012 model (solid curves in the top panel), illustrating that N-2003 has a harder spectrum than source B. The *Chandra* spectrum of N-2003 can be fit well by an absorbed power law with $N_H \approx 2.8 \times 10^{23}$ cm^{-2} and $\Gamma \approx 1.9$ (dashed curve in the top panel), which differs from the $\Gamma \approx 3.1$ slope of source B.

(A color version of this figure is available in the online journal.)

epoch 2). We note that the morphology of the diffuse 3–8 keV *Chandra* emission in the nuclear region is complex and appears brightest in the immediate vicinity of N-2003 and source B (see Figures 2(b)–(e)). As such, detailed modeling of the background spectrum associated with the diffuse emission in this region is difficult. To mitigate this limitation, we restricted our *Chandra* spectral analysis to energies above 3 keV to exclude strong continuum contributions from the hot interstellar medium (ISM) and added an Fe component at 6.7 keV to account for the gas emission line (see Section 3.1 for motivation). Given that the *NuSTAR* difference spectra of source B do not show a strong Fe line (see Figure 3(b)), we do not expect that this component is intrinsic to source B; however, we are less certain about the nature of the Fe line associated with N-2003. The best-fitting spectral model for source B, presented in Section 3.1, renormalized to the 3–5 keV flux of N-2003, is obviously far too steep to fit the higher-energy 5–8 keV spectrum of N-2003, supporting the conclusion that source B and N-2003 are different, despite having similar 2–10 keV fluxes. As a caveat, we note that X-ray binaries accreting at near-Eddington rates can have variable spectral properties without substantial changes in luminosity (e.g., GRS 1915+105; Vierdayanti et al. 2010), implying that the harder spectrum of N-2003 does not rule out a ULX origin similar in nature to source B. The *Chandra* spectrum of N-2003 can be fit well using an absorbed power-law model with $N_H = (2.8 \pm 0.6) \times 10^{23}$ cm^{-2} and $\Gamma = 1.9 \pm 0.6$, and an Fe line fixed at 6.7 keV. If we used only the *Chandra* data to fit the spectrum of source B, we find $N_H = (1.9 \pm 0.8) \times 10^{23}$ cm^{-2} and $\Gamma = 3.1 \pm 1.0$, consistent with the values found from our *NuSTAR* analysis in Section 3.2. Although the fitting parameters of N-2003 and source B are formally consistent, the spectrum of N-2003 is harder than that of source B (see bottom panel of Figure 5), and more consistent with an AGN ($\Gamma \approx 1.5$–2.2; see further discussion above).

Due to its close proximity to the dynamical center and its harder spectrum, it is plausible that N-2003 is an AGN that was in a low state during our 2012 monitoring campaign. However, we cannot currently rule out a ULX nature for N-2003. If N-2003 were an AGN, the $\Gamma \approx 1.9$ power-law spectrum would extend well into the *NuSTAR* bandpass out to beyond ≈ 40 keV. The observed 2–7 keV flux of N-2003 is 1.1 times that of source B in epoch 2. However, if N-2003 were an AGN, then we predict that it would have had a 10–20 keV flux $\gtrsim 2.5$ times higher than that of source B at its peak in epoch 2. Therefore, future monitoring of NGC 253 with both *Chandra* and *NuSTAR* would be able to resolve the degeneracy between the AGN and ULX nature of N-2003 if caught in a high state.

4. SUMMARY

We performed nearly simultaneous *NuSTAR* and *Chandra* monitoring of the nearby starburst galaxy NGC 253 over three observational epochs: beginning 2012 September 1, 2012 September 15, and 2012 November 16. We find that the 7–20 keV nuclear region flux was elevated over the epoch 1 level by factors of ≈ 1.7 and ≈ 1.4 in epochs 2 and 3, respectively. Our *Chandra* observations show that a single variable source, which we call source B (see Figures 2(b)–(e)), was responsible for driving this variation. The *NuSTAR* difference spectra (i.e., subtracting epoch 1 from the bright states in epochs 2 and 3) allows us to study the spectrum of source B over the 3–20 keV energy range. Source B has a peak observed 2–10 keV luminosity of $\approx 1.4 \times 10^{39}$ erg s^{-1} (estimated unabsorbed, intrinsic $L_{2-10\,keV} \approx 5.1 \times 10^{39}$ erg s^{-1}) and is fit well by a broken power-law model with spectral slopes and a break energy within the range of values characteristic of ULXs and not AGNs.

A previous *Chandra* observation in 2003 revealed a hard X-ray source "N-2003" that had a similar 2–7 keV flux to that observed for source B in epoch 2; however, the position of N-2003 is displaced from source B by ≈ 1 arcsec. The high-precision imaging of *Chandra* allows us to show at the $\gg 99.99\%$ confidence level that N-2003 is unrelated to source B. Further examination of the position of N-2003 indicates that it is a better AGN candidate than source B; however, the *Chandra* spectrum alone cannot rule out that N-2003 may be a second ULX. We predict that if N-2003 were an AGN, then a *NuSTAR* observation would have yielded a 10–20 keV flux that was $\gtrsim 2.5$ times higher than that of source B at its peak brightness. In light of this, future monitoring with *Chandra* and *NuSTAR* would be able to break the degeneracy between a ULX and AGN nature of N-2003, if it returns to a bright state.

REFERENCES

Arnaud, K. A. 1996, in ASP Conf. Ser. 101, Astronomical Data Analysis Software and Systems V, ed. G. Jacoby & J. Barnes (San Francisco, CA: ASP), 17
Bauer, M., Pietsch, W., Trinchieri, G., et al. 2007, A&A, 467, 979
Bauer, M., Pietsch, W., Trinchieri, G., et al. 2008, A&A, 489, 1029
Brunthaler, A., Castangia, P., Tarchi, A., et al. 2009, A&A, 497, 103
Corral, A., Della Ceca, R., Caccianiga, A., et al. 2011, A&A, 530, A42
Fabbiano, G., & Trinchieri, G. 1984, ApJ, 286, 491
Feng, H., & Kaaret, P. 2007, ApJ, 668, 941
Fernández-Ontiveros, J. A., Prieto, M. A., & Acosta-Pulido, J. A. 2009, MNRAS, 392, L16
Gladstone, J. C., Roberts, T. P., & Done, C. 2009, MNRAS, 397, 1836
Hammer, F., Puech, M., Chemin, L., Flores, H., & Lehnert, M. D. 2007, ApJ, 662, 322
Harrison, F. A., Craig, W. W., Christensen, F. E., et al. 2013, ApJ, 770, 103
Heil, L. M., Vaughan, S., & Roberts, T. P. 2009, MNRAS, 397, 1061
Hofner, P., Baan, W. A., & Takano, S. 2006, AJ, 131, 2074
Karachentsev, I. D., Karachentseva, V. E., Huchtmeier, W. K., & Makarov, D. I. 2004, AJ, 127, 2031
Kim, M., Kim, D.-W., Wilkes, B. J., et al. 2007, ApJS, 169, 401
Mineo, S., Gilfanov, M., & Sunyaev, R. 2012, MNRAS, 419, 2095
Mitsuishi, I., Yamasaki, N. Y., & Takei, Y. 2011, ApJL, 742, L31
Mitsuishi, I., Yamasaki, N. Y., & Takei, Y. 2013, PASJ, 65, 44

Müller-Sánchez, F., González-Martín, O., Fernández-Ontiveros, J. A., Acosta-Pulido, J. A., & Prieto, M. A. 2010, ApJ, 716, 1166
Pence, W. D. 1980, ApJ, 239, 54
Pietsch, W., Roberts, T. P., Sako, M., et al. 2001, A&A, 365, L174
Pietsch, W., Vogler, A., Klein, U., & Zinnecker, H. 2000, A&A, 360, 24
Ponti, G., Terrier, R., Goldwurm, A., Belanger, G., & Trap, G. 2010, ApJ, 714, 732
Ptak, A., Serlemitsos, P., Yaqoob, T., Mushotzky, R., & Tsuru, T. 1997, AJ, 113, 1286
Roberts, T. P. 2007, Ap&SS, 311, 203
Rodríguez-Rico, C. A., Goss, W. M., Zhao, J.-H., Gómez, Y., & Anantharamaiah, K. R. 2006, ApJ, 644, 914
Shemmer, O., Brandt, W. N., Netzer, H., Maiolino, R., & Kaspi, S. 2006, ApJL, 646, L29
Stark, A. A., Gammie, C. F., Wilson, R. W., et al. 1992, ApJS, 79, 77
Strickland, D. K., Heckman, T. M., Weaver, K. A., & Dahlem, M. 2000, AJ, 120, 2965
Ulvestad, J. S., & Antonucci, R. R. J. 1997, ApJ, 488, 621
Vasudevan, R. V., Brandt, W. N., Mushotzky, R. F., et al. 2013, ApJ, 763, 111
Vasudevan, R. V., & Fabian, A. C. 2007, MNRAS, 381, 1235
Vierdayanti, K., Mineshige, S., & Ueda, Y. 2010, PASJ, 62, 239
Vogler, A., & Pietsch, W. 1999, A&A, 342, 101
Weaver, K. A., Heckman, T. M., Strickland, D. K., & Dahlem, M. 2002, ApJL, 576, L19
Younes, G., Porquet, D., Sabra, B., & Reeves, J. N. 2011, A&A, 530, A149